research on the dynamic loading characteristics is less at home and abroad. Moreover as the homogeneous sand or sand soil was used in many testes, the experimental research of reinforcement cohesive soil is reported not more so far. In this paper, the dynamic triaxial test of reinforcement cohesive soil has been done, and its dynamic strength and deformation law of development in the cycle dynamic loading has been analyzed.

TEST EQUIPMENT AND METHOD

The test equipment is the electro-hydraulic servo soil dynamic triaxial test machine (SDT 100 model) made by Xian Lichuang Measuring Instrument Co. The samples used of soil are from a reconstruction place in the Mianyan Road in Sichuan province. The samples is low liquid limit silty clay which color is brown yellow and specific gravity is 2.72. Their liquid limit is 42.8%, plastic limit 27.2% and plastic index is 15.6%. The most optimum moisture content is 13.7% and the maximum dry density is 1.8 g/m^3. The diameter of the prepared samples in the optimum moisture content is 61.8mm, height 125mm. The reinforcement material is the warp knitting geogrid reinforced materials in the Mianyan road whose grid size is 21.0mm x 21.0mm, the mass in unit area is 447g/m^2, longitudinal tensile strength is 63.4KN/m and the elongation is 2.80%, transverse tensile strength is 74.5KN/m and the elongation is 2.90%. The materials are arranged and layered horizontally, which a reinforcement layer is in the central part of the sample, and two reinforcement layers are respectively placed in a third place in the sample. The samples are prepared in strict accordance with the soil test execution procedures, and the sample moisture content and density are controlled strictly in the test.

The vehicle dynamic load is simulated with the approximate sine load in the test. The value of vibration frequency refer to the results of related literature, and the test vibration frequency is 1.0Hz. Considering the characteristics of geosynthetic reinforcement engineering and the safety of test results in engineering application, the unconsolidated undrained test (UU test) is adopted. Because of lack of research on cohesive soil reinforcement dynamic load tests, the methods of fatigue-dynamic tests of some rock under dynamic loading are referred. Before this dynamic triaxial test, the static triaxial test based on the same density and the moisture content is done in order to sure the static strength. The stress values in the center of vibration of the dynamic test are the 0.6 times of the static strength values under the corresponding condition. The confining pressures of dynamic test are 100, 200 and 300KPa respectively, The tests of 3 ~ 4 samples are carried on under each confining pressure. Considering the properties of cohesive soil engineering, the failure strain in standard is used in the test that if the cumulative axial strain is up to 5%, the sample is thought failed. The pausing condition of the test is the axial strain more than 5% and the most vibration time is 3000 times.

DYNAMIC SHEAR STRENGTH ANALYSIS

The data collected of the experiment is processed, and dynamic shear strength curves(τ_d - $lg\ N_f$) are drawn and fitted to get dynamic strength curve equation.

Dynamic Shear Strength Curve

It can be known from different reinforced geogrid layers in different confining pressure tests of dynamic shear strength curve(Figure 1) that whether the confining pressure is 100，200 or 300KPa, the change rule of dynamic shear strength curve is nearly same that the curve is steep overall in the early stage of vibration, then it tends to be flattened with vibrations time increasing; the permutation of the curves from top to down is always made up two layers the reinforcement, a layer the reinforcement and soil(not the reinforcement). The test results show that: (1) The geogrid layers on reinforcement of the cohesive soil have obvious influence on the dynamic strength. No matter that the reinforcement a layer or two layers, the dynamic stress of reinforced soil required is far greater than that of the soil to achieve the same damage strain in the same cycle times which shows that the reinforced soil has a good ability in ant-vibration and reinforced material in the arrangement of the cohesive soil can improve the grid soil shear strength, reduce the dynamic soil deformation; (2) With other conditions being the same as the more reinforcement layers, the dynamic shear strength is the greater and the reinforcement effect is the better, taking confining pressure 200KPa as an example, vibration time of the damage being 50 times, the dynamic shear strength of the two reinforcement layers increases about 55% and the dynamic shear strength of the one reinforcement layer increases more about 30% than that of soil (not the reinforcement); (3) The reinforcement effect on the dynamic strength in high confining pressure is better, taking an example, to achieve the same damage strain, the dynamic stress with confining pressure being 300KPa is far bigger than that with 100KPa and 200KPa for different geogrid layers on the same cycle times; (4) The dynamic stress amplitude on the reinforcement soil destruction has significant effects on the number of vibration. under the same confining pressure, the deformation of the sample whose dynamic stress amplitude is bigger in high cycle load increases soon, while the sample can be damaged in smaller time of the vibration, and vice versa.

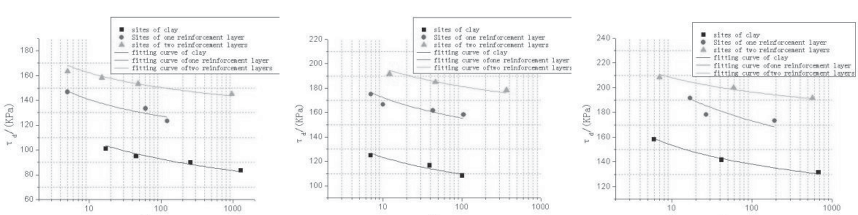

(a) σ_3=100KPa (b) σ_3=200KPa (c) σ_3=300KPa

FIG. 1. The dynamic strength curve of different confining pressure.

Dynamic Shear Strength Fitting Curve Equation

The test results of dynamic shear stress and damage of the vibration time are fitted and it is found that dynamic shear stress and damage of the vibration times with logarithmic function fitting the better, fitting equation can be written as:

$$\tau_d = ALn\ (-BLnN_f)$$

In the function, τ_d is the dynamic shear stress in failure; N_f is vibration times of the corresponding destruction; A and B are the fitting parameters of the equation which are related to the category of soil, the reinforcement layer, the initial stress state and the dynamic stress on amplitude. The parameters in the function of the shear strength curve see Table 1.

Table 1. The Dynamic Strength Curve Fitting Test Results

Sample state	σ_3 (KPa)	A	B	R^2
	100	-22.647	-0.00363	0.91107
No reinforcement	200	-20.419	-0.00102	0.91515
	300	-22.813	-5.11078E-4	0.98551
One	100	-19.049	-2.7151E-4	0.90729
reinforcement	200	-24.186	-3.50218E-4	0.71965
layer	300	-36.649	-0.00192	0.67531
Two	100	-16.361	-2.24521E-5	0.90036
reinforcement	200	-21.361	-4.45533E-5	0.84680
layers	300	-16.891	-1.92364E-6	0.92957

For 0 ~ 2 layer reinforcement, their R^2 value are respectively in 0.92 ~ 0.98, 0.68 ~ 0.91 and 0.85 ~ 0.93, and it can explain that the degree of fitting of test data is good. Through putting the damaged vibration time in the test into the fitting formula to calculate the dynamic shear stress of the experiment and calculating and analyzing the dynamic shear stress absolute error, the absolute error range of the soil is between 0.81% ~ 2.79%, the absolute error of one reinforcement layer between 0.33% ~ 4.03%, the absolute error of two reinforcement layers between 0.01% ~ 3.60%. Because fitting parameters are obtained through the test, fitting formula is useful to practical application.

DEFORMATION ANALYSIS

Relationship Between Axial Strain Accumulation and Vibration Time

The development of deformation of the soil in the dynamic loading is in connection with the dynamic stress.

In the test it is found that when the dynamic stress is less than the damage loads, the deformation of samples can not reach its failure strain. In Figure 2 it can be seen that the accumulation axial strain of reinforcement increases with the vibration time increasing, and in the earlier period of the vibration, when the time is 300 or so, accumulation of axial strain increases fast with vibration time increasing as almost linear increasing, and the strain can achieve 60% ~ 70% of total strain. With the vibration time increasing, the increased rate of axial strain becomes very small and axial strain increment is very slow and axial strain accumulation becomes stable. This deformation law of the reinforcement is consistent with that of cohesive soil under dynamic loading.

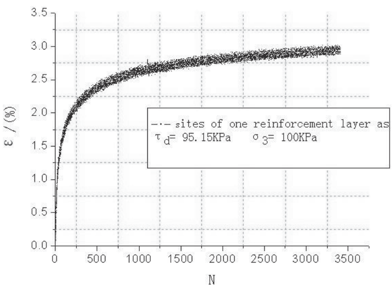

(a) one reinforcement layer as τ_d =95.15Kpa, σ_3=100KPa

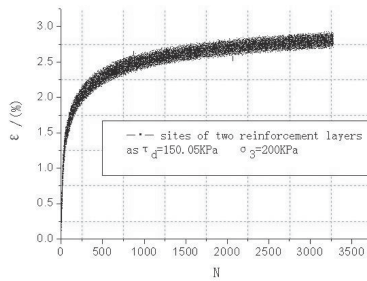

(b) two reinforcement layers as τ_d=150.05Kpa, σ_3=200KPa

FIG. 2. The relation curves between axial cumulative strain and vibration times.

When the dynamic stress applied is more than dynamic destruction loads, soil samples will be damaged due to big deformation. In Figure 3 it can be seen that when the dynamic stress is bigger than critical dynamic stress, the axial accumulated strain of the reinforcement also increases with the increase of the vibration time. And in the initial about 50 times vibration, the axial strain accumulation can reach 60% ~ 70% of the damage strain; in 100 ~ 200 times vibration, the increased speed of axial accumulative strain is small with nonlinear increase overall, and the deformation of samples can not stable; the axial strain will accumulate more than 5% so that the sample is damaged due to bigger deformation finally.

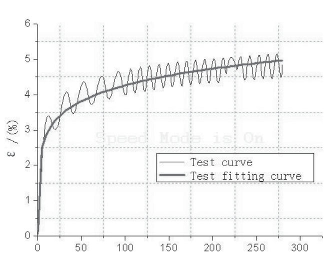

(a) one reinforcement layer as τ_d =173.36Kpa, σ_3=300KPa

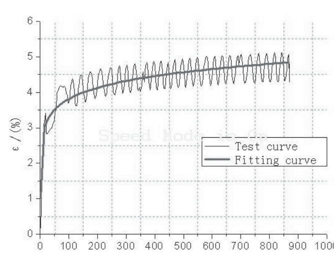

(b) two reinforcement layers as τ_d =191.69Kpa, σ_3=300KPa

FIG. 3. The relation curves between axial cumulative strain and vibration times.

In Figure 2 and Figure 3, the relationship of axial strain accumulation and vibration time was fitted, and fitting function is:

$$\varepsilon_p = A + BN^C$$

In the function, the ε_p is cumulative plastic strain; N is times of cycle load; A , B and C are the fitting parameters of the equation which are related to the category of soil, the reinforcement layer, the initial stress state and the amplitude of the dynamic stress. The fitting parameters of the sample in Figure 2 and Figure 3 are shown in Table 2.

Table 2 Fitting test results

Parameters	A	B	C	R^2
Value	0	0.94947	0.14269	0.90680
	0	0.93441	0.13964	0.87129
	-4.11446	5.82996	0.07876	0.80926
	-2.57656	4.65449	0.06889	0.75496

The Relationship between Axial Strain Accumulation and Geogrid Layers

Geogrid layers to axial accumulated strain have significant effect. In the same confining pressure and dynamic load conditions, the axial accumulative strain decreases as the increase of geogrid layers. Taking an example, when confining pressure is 200KPa and dynamic shear stress is 108.35KPa, the soil (not the reinforcement) will be failed and the axial strain will be accumulated 5.63% as the vibration times is only 200, but reinforced layers is not damaged in the end of test outage, and the axial strain accumulation is only 2.78%(one reinforced layer) and 0.92%(two reinforced layers). The final cumulative axial strain is only 49.3% and 16.3% of the soil (not the reinforcement) respectively. That means that reinforced soil has good ability in ant-vibration, and arranging geogrid into cohesive soil is a feasible method to improve the dynamic strength of soil, to restrain the axial strain and reduce the accumulation of settlement and deformation.

Relationship between Axial Strain and Dynamic Stress Amplitude

Dynamic stress amplitude has great influences on the axial strain. The relationship between the axial strain of different reinforced geogrid layers and vibration time has similarity. The influence of dynamic stress amplitude to axial cumulative plastic strain is explained using relation curve of the axial accumulated strain of one reinforcement layer with 300KPa confining pressure and different dynamic stress.

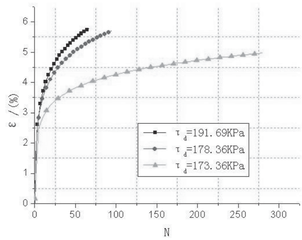

One reinforcement layer as
σ_3=300KPa

FIG. 4. The relation curves between axial cumulative plastic strain and vibration times.

In Figure 4 it can be seen that the dynamic stress has great influence on the axial strain accumulation of the reinforcement, and this is similar to the influence of dynamic stress to dynamic strength. Whether or not the reinforcement, the axial strain accumulation increases with the increase of the dynamic stress and vibration time of reaching damaged strain is smaller. This is because each cycle strain energy can be directly related to stress amplitude. When dynamic stress amplitude is greater, the energy in the development of deformation is more, and the development of deformation is faster, and vibration time needed is also less.

CONCLUSIONS

In view of this experiment, the following conclusions may be drawn.

(1) The dynamic strength of reinforced soil shows good regularity as the amplitude of dynamic stress and reinforced geogrid layers change, and the forms of dynamic strength curve of reinforced soil are basically uniform with different conditions. The dynamic strength curve can be expressed as $\tau_d = A\ Ln\ (-B\ Ln\ N_f)$;
(2) The axial cumulative strain increases quickly with vibration times increasing under cyclic loading during the earlier stage of the vibration which can reach 60% ~ 70% of the total strain, and it remains stable with vibration times increasing if the dynamic stress is smaller than the limited dynamic stress; But the axial cumulative strain increases slower than it during the earlier stage and it was nonlinear totally if the dynamic stress is bigger than the limited dynamic stress and the sample fails eventually for instability;
(3) The development of the axial accumulated strain of reinforcement shows good regularity along with dynamic stress amplitude and geogrid layers change whose relationships may be described as $\varepsilon_p = A + B\ N^C$.

REFERENCES

Cai, Y. and Cao, X. W. (1996). "Repeated load subgrade soil under the critical dynamic stress and permanent deformation discussed." *J. Southwest Jiaotong*

University, v.31 (1): 1-5.

Fu, H., Ling, H., and Cai, Z. Y. (2008). "The experimental research on the factors of reinforced strength." *J. Geotechnical Mechanics*, v.28 (s1): 481-484.

Ge, X. R., Jiang, Y., Lu, Y. D., and Ren, J. X. (2003). "Cycle load rock deformation characteristics of the experimental studies." *J. Fatigue Rock Mechanics and Engineering*, v22 (10): 1581 - 1585.

He, J. Q., Yang, J. S., and J, M. (2008). "The cycle load soil mechanical properties with coal gangue experimental study." *J. Rock Mechanics and Engineering*, v. 27 (1): 199-205.

Peng, S. Q., Zhao, J, H., and Huang, R. Q. (2002). "Chengdu clay dynamic triaxial test research." *J. Geological Hazard and Environmental Protection*, v. 13 (1): 57-60

Ren, J. X., Jiang, Y., and Ge, X. R. (2005). "Uniaxial compressive rock fatigue life influence factors were analyzed." *J. Chinese Journal of Geotechnical Engineering*, v. 27 (11): 1282 - 1285.

Song, X. Y., Luo, R. A., Shan, Y. F., and Cheng, C. J. (2003). "Rock and elastic-plastic fatigue strength test theory analysis preliminary studies." *J. Geotechnical Engineering*, v. 24 (s2): 171 -174.

Wu, J. H. (2000). "Geosynthetic materials reinforcement sandy soil test." *J. of Geotechnical Engineering*, v. 22 (2): 200-204.

Xie, W. L., Xue, J. G., and Chang, B. (2008). "Reinforced the dynamics characteristics of triaxial test." *J. Science*, v. 23 (B9): 120 - 124.

Yang, P., Ye, W. M., and Zhang, Y. W. (2009). "Train for power load power subgrade soil deformation analysis." *J. of Underground Space and Engineering*, v. 5 (6): 1166-1169.

Yang, Y., Bai, S., and Zhang, J. (2009). "Reinforced the dynamic triaxial test." *J. of Subgrade Engineering Study*, (5): 178-179.

Zhang, M. X., & Min, X. (2006). "The three-dimensional soil reinforcement. Single characters of triaxial test study." *J. of Geotechnical Engineering*, v. 28 (8): 931-936.

A Numerical Study on Artificial Fill Embankment with Liquefiable Foundation Using FLAC

Genlong Wang[1], S.M. ASCE, Hengxing Lan[2] and Guoqiang Yu[3]

[1]Associate professor, Xi'an Center of Geological Survey, China Geological Survey, No. 438, East of Youyi Road, Beilin District, Xi'an 710054, China; wang2006@mail.iggcas.ac.cn
[2]Researcher, Institute of Geographic Sciences and Natural Resources Research, Chinese Academy of Sciences, 11A, Datun Road, Chaoyang District, Beijing 100101, China; lanhx@lreis.ac.ca
[3]Assistant researcher, Xi'an Center of Geological Survey, China Geological Survey, No. 438, East of Youyi Road, Beilin District, Xi'an 710054, China; yuguoqiang23@163.com

ABSTRACT: The problem of seismic liquefaction related to artificial fill embankment is complicated. In this study, by making using of Finn model, a typical artificial fill embankment was simulated by means of Finn model in FLAC. Numerical simulation results indicated that the pore water pressure of saturated sand soil increased extremely which resulted in the significant decrease of the effective stress. When the effective stress decreased approximately to zero, the liquefaction phenomena occurred. According to the change of pore water pressure at different locations and depths, three rules have been obtained. Firstly, the occurrence time for the first peak of pore water pressure coincided with the seismic peak acceleration of input wave. Secondly, the liquefaction occurred earlier in the upper-layer of saturated sand soil than in the lower-layer below the bottom of slope. However the duration of liquefaction in lower-layer of saturated sand soil was longer than in the upper-layer. Thirdly, the upper-layer of saturated sand soil was almost not liquefiable below the top of slope, while the lower-layer was easily liquefiable with long time duration. In summary, the characteristics of seismic liquefaction in the artificial fill embankment were closely related to the seismic wave, locations and depths of saturated sand soil in a slope.

INTRODUCTION

Earth embankments are constructed for various purposes, such as river dykes, earth dams and road embankments. A large number of earth embankments are prone to partial or total damage, mainly due to the liquefaction of the embankments and/or foundation soils induced by earthquakes (Adalier and Sharp, 2004; Huang et al., 2008), i.e. in the 1975 Tangshan earthquake in China (Fu and Zeng, 2005; Chen et al., 2009), the 1995 Hyogoken–Nambu Earthquake in Japan (Matsuo, 1996), the 1995 Kobe earthquake in Japan, the 1999 Chi-chi earthquake in Taiwan, the 2001 Bhuj Earthquake in India (Krinitzsky and Hynes, 2002) and the 2008 Wenchuan earthquake in China (Zhou et al., 2009; Wang et al., 2013). Earthquake-triggered liquefaction may cause a significant loss of strength of the soil mass with a progressive build-up of pore pressure, resulting in large permanent deformation and even complete failure of the embankments (e.g. Seed et al., 1985; Wang et al., 2010).

Experimental tests and numerical simulation are two major approaches to analyze the stability of earth embankments under earthquake loading. Experimental tests related to these problems include shaking table tests (Koga and Matsuo, 1990; Park et al., 2000) and dynamic centrifuge tests (Koseki et al., 1994; Adalier et al., 1998). Because of high cost for experimental test, the numerical simulation becomes the most useful alternative approach. Numerical simulation approaches have many advantages over physical experimental methods. They can rapidly and efficiently change test conditions and component properties without inordinate setup costs or significant downtime. Numerical simulations for engineering practice have been applied by an increasing number of researchers, especially with advances in computer technology. They have been widely used to solve specific problems of earth embankments under earthquake loading in the past few decades. Pekau and Cui (2004) carried out a comprehensive study of the dynamic behavior of the fractured Koyna dam in India during earthquakes using the distinct element method (DEM). Siyahi and Arslan (2008) used finite element to analyze the dynamic behavior, failure modes and mechanisms of failure of the dam under ground motions. Huang et al. (2012) studied the seismic performance in a numerical model to examine the effect of anti-liquefaction treatments on liquefaction foundation soils during earthquake loading.

This work aims to investigate the characteristics of the accumulation and dissipation for pore water pressure under earthquake loading and the subsequent liquefaction in an artificial fill embankment. The results are valuable to the understanding of liquefaction mechanism in the seismic area.

2. METHODOLOGY

2.1 Finn model

The Finn model for liquefiable soil was employed in this study. This mechanism was well-described by Martin et al. (1975). The empirical equation, which indicates the relation between the increment of volume and shear strain, is given as:

$$\Delta\varepsilon_{vd} = C_1(\gamma - C_2\varepsilon_{vd}) + \frac{C_3\varepsilon_{vd}^2}{\gamma + C_4\varepsilon_{vd}} \tag{1}$$

where $\Delta\varepsilon_{vd}$ is the increment of volume, ε_{vd} is the accumulated irrecoverable volume strain, γ is shear strain, C_1, C_2, C_3 and C_4 are constants.

Bryne (1991) proposed an alternative and simpler formula on the basis of Martin's research. It is expressed as:

$$\frac{\Delta\varepsilon_{vd}}{\gamma} = C_1 \exp\left(-C_2 \frac{\varepsilon_{vd}}{\gamma}\right) \tag{2}$$

where C_1 and C_2 are constants with different interpretations from those of Eq. 2. In many cases, C_2=0.4/C_1, so Eq. 2 involves only one independent constant.

Bryne noted that the constant, C_1, can be derived from relative densities, D_r, as follows:

$$C_1 = 7600(D_r)^{-2.5} \tag{3}$$

Further, using an empirical relation between D_r and normalized standard penetration test value $(N_1)_{60}$:

$$D_r = 15\sqrt{(N_1)_{60}} \tag{4}$$

Substituting Eq. 4 into Eq. 3, then,

$$C_1 = 8.7(N_1)_{60}^{-1.25} \tag{5}$$

2.2 Geological model and boundary conditions

According to engineering geological conditions of the fill embankment, the geological model has been simplified as a fill layer, a sand soil layer and a gravel soil layer (see in FIG. 1). The model size has been set to three times the actual size of the embankment for the purpose of decreasing boundary effects. The numerical model was 35 m high and 155 m wide, with 1510 quadrilateral elements. The thickness of sand soil layer (i.e., liquefiable soil) was 12 m, and the gravel soil layer was 18 m. The water table was 1.5 m below the surface.

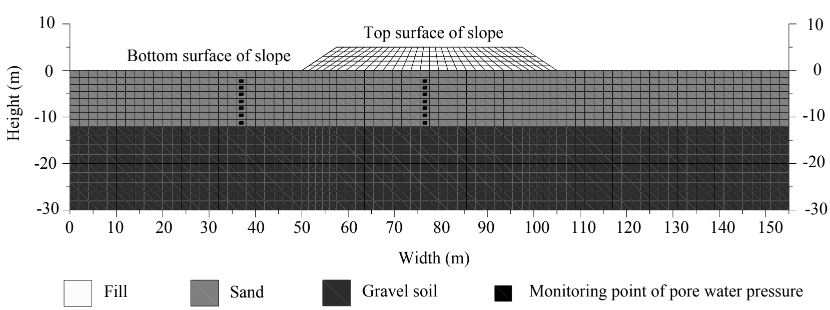

FIG. 1 The model of numerical simulation for the embankment.

FLAC dynamic numerical simulation has strict requirements for element size. The size must be smaller than approximately one-tenth to one-eighth of the wavelength